Journal Pre-proof

Untargeted metabolomics reveals the role of AQP9 in nonalcoholic fatty liver disease in a mice model

Quancheng Cheng, Junwei Zhang, Jinyu Fang, Huiru Ding, Yiyao Xu, Xin Lu, Weiguang Zhang

PII: S0141-8130(22)01716-0

DOI: https://doi.org/10.1016/j.ijbiomac.2022.08.023

Reference: BIOMAC 21686

To appear in: *International Journal of Biological Macromolecules*

Received date: 7 July 2022

Revised date: 2 August 2022

Accepted date: 5 August 2022

Please cite this article as: Q. Cheng, J. Zhang, J. Fang, et al., Untargeted metabolomics reveals the role of AQP9 in nonalcoholic fatty liver disease in a mice model, *International Journal of Biological Macromolecules* (2022), https://doi.org/10.1016/j.ijbiomac.2022.08.023

Title page:

Title: Untargeted Metabolomics Reveals the role of AQP9 in Nonalcoholic Fatty Liver Disease in a Mice Model

Quancheng Cheng[a, 1], Junwei Zhang[b, 1], Jinyu Fang[a], Huiru Ding[a], Yiyao Xu[b, ***], Xin Lu[b, **], Weiguang Zhang[a, *]

[a] Department of Human Anatomy and Histology and Embryology, School of Basic Medical Sciences, Peking University Health Science Center, Beijing 100191, China

[b] Department of Liver Surgery, State Key Laboratory of Complex Severe and Rare Diseases, Peking Union Medical College (PUMC) Hospital, Chinese Academy of Medical Sciences and Peking Union Medical College, Beijing, 100730, China.

[*] Corresponding author: Weiguang Zhang, Department of Human Anatomy and Histology and Embryology, School of Basic Medical Sciences, Peking University, Beijing 100191, China. Email: zhangwg29@163.com

[**] Corresponding author: Xin Lu, Department of Liver Surgery, State Key Laboratory of Complex Severe and Rare Diseases, Peking Union Medical College (PUMC) Hospital, Chinese Academy of Medical Sciences and Peking Union Medical College, Beijing, 100730, China. Email: China_luxin@pumch.cn

[***] Corresponding author: Yiyao Xu, Department of Liver Surgery, State Key Laboratory of Complex Severe and Rare Diseases, Peking Union Medical College (PUMC) Hospital, Chinese Academy of Medical Sciences and Peking Union Medical College, Beijing, 100730, China. Email: xuyiyao@hotmail.com

[1] These authors contributed equally: Quancheng, Cheng, Junwei Zhang.

Abstract:

Previous studies have shown that AQP9 plays an important role in energy metabolism in nonalcoholic fatty liver disease (NAFLD). Recently, metabolomic analyses were used to determine the slight changes in metabolic profiles and helped to understand the disease progression, therapeutic intervention of NAFLD. A mouse model of NAFLD was established with a high-fat diet (HFD), and *Aqp9* knockout mice were constructed. Untargeted metabolomics techniques were used to evaluate the potential mechanism of the effect of AQP9 in NAFLD. The results indicated that AQP9 plays a regulatory role in the occurrence of NAFLD. Moreover, a total of 220 candidate

biomarkers were screened and identified. Cluster analysis and enrichment analysis of differential metabolites indicated that fatty acid biosynthesis was mainly disturbed when compared against the control group, which was mitigated by knockout of *Aqp9*. These results show that untargeted metabolomics help to understand the effects of AQP9 in NAFLD.

Keywords: nonalcoholic fatty liver disease; aquaporin 9; untargeted metabolomic

Abbreviations

NAFLD Nonalcoholic fatty liver disease

T2DM type 2 diabetes mellitus

AQP9 aquaporin 9

AQPs aquaporins

HFD high-fat diet

NFD normal fat diet

PCR Polymerase chain reaction

TC total cholesterol

TG triglyceride

LDL-C low-density lipoprotein cholesterol

HDL-C high-density lipoprotein cholesterol

AST aspartate aminotransferase

ALT alanine aminotransferase

HE hematoxylin and eosin

ORO Oil Red O

SOD superoxide dismutase

GSH-Px glutathione peroxidase

MDA malondialdehyde

ELISA wnzyme linked immunosorbent assay

IL-6 interleukin-6

IL-1β interleukin-1β

TNF-α tumor necrosis factor-α

QC quality control

PCA principal component analysis

OPLS-DA orthogonal partial least-square discriminant analysis

VIP variable importance on projection

NASH nonalcoholic steatohepatitis

Introduction

Nonalcoholic fatty liver disease (NAFLD) is acknowledged to be the leading chronic liver disease[1], presenting an increasing incidence worldwide[2]. NAFLD not only causes liver-related morbidity and mortality by increasing the risk of hepatocellular carcinoma and cirrhosis but also is reported to be a multisystem disease, with an increased risk of type 2 diabetes mellitus (T2DM), cardiovascular disease, and chronic kidney disease[3, 4]. However, the pathogenesis of NAFLD is largely unknown, and no pharmacological therapies have been approved to prevent or treat NAFLD to date[5]. Therefore, there is pressing need to study the mechanisms of NAFLD development and to find effective and safe treatments for this important clinical problem[6].

Aquaporin 9 (AQP9), an aquaporin (AQP), is highly expressed in both human and mouse liver and is involved in the transport of glycerol and other small solutes[7, 8]. Previous studies have shown that AQP9 plays an important role in energy metabolism and serves as an important factor in NAFLD[9-11]. Knockdown of *Aqp9* is able to alleviate high-fat diet (HFD)-induced NAFLD[12, 13]. AQP9 may represent a novel target of NAFLD that may antagonize its progression by reducing lipotoxicity in the liver[14]. It is of great translational value to study the function of AQP9 in NAFLD. The available information about AQP9 involvement in the pathogenesis of NAFLD is limited to the evaluation of transcript levels without functional data[13, 15].

Metabolomics, which is the profiling of metabolites in biofluids, cells, and tissues, is now capable of providing insight into the mechanisms of biological pathways[16]. Metabolomic analyses could help to determine the slight changes in metabolic profiles and to understand disease progression and therapeutic intervention[17, 18]. Hence, the aim of the present study was to use untargeted metabolomics to examine the effect of AQP9 in the development of NAFLD and the role of knockout of *Aqp9* in

treating NAFLD. The results of this study suggest that AQP9 serves as a novel molecular target for therapeutic intervention in NAFLD by downregulating lipid-related metabolites.

Methods

1. Mouse preparation and sampling

Aqp9$^{-/-}$ mice were supplied by Peking University, and the method was described previously[14]. Genotype identification results of *Aqp9*$^{-/-}$ mice were shown in Figure S1. Wild-type mice (C57BL/6) were purchased from the Peking University Health Science Center Department of Laboratory Animal Science. The mice were housed under a 12-hour light-dark cycle in a thermostatically controlled barrier facility with free access to food. The mice were deeply anaesthetized with isoflurane and then sacrificed. For all experiments, a minimal number of animals were used and pain was minimized to the bestest extent possible. This study was approved by the Local Ethics Committee for Animal Research Studies at the Peking University Health Science Center, No. LA2017100. A total of 24 mice were divided into four groups: wild-type normal fat diet (NFD) (WT-Control); *Aqp9* knockout NFD (KO-Control); wild-type HFD (WT-HFD); and *Aqp9* knockout HFD (WT-Control), as shown in Figure S2. NFD (D12450K, Research Diets, NJ, USA) was composed of 10% fat-derived calories, while HFD (D12492, Research Diets, NJ, USA) had 60% fat-derived calories. All mice were bred with NFD for 29 weeks and weighed approximately 20-25 g, followed by NFD or HFD for the next 12 weeks. Body weight was observed weekly.

2. Genotype identification

The tail tips of 20-day-old mice were disinfected with 75% alcohol, and tail tissues of 1–3 mm were cut with surgical scissors. Next, 50 μL of DNA extraction fluid (Table 1) was added after the tissues were completely digested in a water bath at 55 °C for 6 – 7 h, and 100 μL of water was added, boiled for 5 min, oscillated on an oscillator for 1 min, and centrifuged at 10,000 revolutions for 4 min. Next, centrifugation was performed at 10000 revolutions for 4 min. Polymerase chain reaction (PCR) of target genes was then performed according to the reaction procedure in Table 2 and reaction system in Table 3. The PCR products were electrophoresed in a 1% agarose gel and then observed and photographed under a UV lamp. The primer sequences used in the experiment are shown in Table 4.

3. Handling of serum samples

At the end of the trial, all animals were anaesthetized after overnight fasting. Six mice per group were analysed. A total of 250 μL of thawed serum samples and 750 μL of prechilled acetonitrile were transferred to 1.5 mL polypropylene tubes, and the mixture was vortexed for 30 s and allowed to stand for 20 min at 4 ◦C before use. The samples were centrifuged at 10,000 rpm for 10 min at 4 ◦C, and the supernatant was transferred into new tubes. Total cholesterol (TC) (E1005), triglyceride (TG) (E1003), low-density lipoprotein cholesterol (LDL-C) (E1018), high-density lipoprotein cholesterol (HDL-C) (E1017), aspartate aminotransferase (AST) (E2023), and alanine aminotransferase (ALT) (E2021) levels were determined according to the manufacturer's instructions (Applygen, Beijing, China) by using a biochemical analyzer (AU5800, Beckman Coulter, USA)

4. Haematoxylin and eosin (HE) staining

After the mice were sacrificed, liver samples were stored in 10% formaldehyde solution and embedded in paraffin. Then, the paraffin sections (4 μm) were dewaxed and rehydrated in differential alcohol gradients for subsequent HE staining to observe histopathological changes by standard light microscopy. HE staining was performed according to the kit's instructions (G1120, Solarbio, Beijing, China).

5. Oil Red O (ORO) staining

Livers were sectioned using a sliding vibratome (CM3050S, Leica, Buffalo Grove, USA) to obtain coronal cryostat sections (20 mm thick). The sections were then stained with ORO following the kit's instructions (G1263, Solarbio, Beijing, China).

6. Liver biochemical analysis

The liver tissues (0.1 g) were weighed and immersed in 900 μl normal saline followed by ultrasonic trituration and centrifugation at 3,000 rpm for 15 min to obtain liver tissue homogenates. The obtained supernatants were used to measure the superoxide dismutase (SOD) (BC0170) and glutathione peroxidase (GSH-Px) (BC1190) activities and the malondialdehyde (MDA) (BC0020) level according to the manufacturer's instructions provided by Solarbio (Beijing, China).

7. Enzyme linked immunosorbent assay (ELISA)

The levels of interleukin-6 (IL-6) (SEKM-0007), interleukin-1β (IL-1β) (SEKM-0002), and tumour necrosis factor-α (TNF-α) (SEKM-0034) in the liver tissue were measured using ELISA according to the manufacturer's instructions provided by Solarbio (Beijing, China).

8. Metabolic profiling with statistical analysis

The changes observed in the metabolites in the liver following knockout of AQP9 for 12 weeks were screened using a UPLC-ESI-Q-Orbitrap-MS system (UHPLC, Shimadzu Nexera X2 LC-30AD, Shimadzu, Japan) coupled with Q-Exactive Plus (Thermo Scientific, San Jose, USA). The detailed protocols used for sample preparation, UPLC–MS, and data analysis are described below.

8.1 Metabolite extraction

Liver samples were weighed before the extraction of metabolites, dry lyophilised and ground in a 2 mL Eppendorf tube containing a 5 mm tungsten bead for 1 min at 65 Hz in a grinding mill. Metabolites were extracted using 1 mL precooled mixtures of methanol, acetonitrile and water (v/v/v, 2:2:1) and then placed for 1 h into ice baths with ultrasonic shaking. Subsequently, the mixture was placed at -20 °C for 1 h and centrifuged at 14,000 × g for 20 min at 4 °C. Additionally, to ensure data quality for metabolic profiling, quality control (QC) samples were prepared by pooling aliquots of all samples that were representative of all samples under analysis, and used for data normalization.

8.2 UHPLC–MS/MS analysis

For hydrophilic interaction liquid chromatography (HILIC) separation, samples were analysed using a 2.1 mm*100 mm ACQUIY UPLC BEH Amide 1.7 μm column (Waters, Ireland). The flow rate was 0.5 mL/min and the mobile phase contained: A: 25 mM ammonium acetate and 25 mM ammonium hydroxide in water and B: 100% acetonitrile (ACN). The gradient was 95% B for 1 min, was linearly reduced to 65% over 7 min, then reduced to 35% over 2 min and maintained for 1 min, and then increased to 95% over 0.5 min, with a 2 min re-equilibration period employed. Both electrospray ionization (ESI) positive mode and negative mode were applied for MS data acquisition. In MS only acquisition, the instrument was set to acquire over the m/z range of 80-1200 Da. The full MS scans were acquired at a resolution of 70,000 at m/z 200 and 17,500 at m/z 200 for the MS/MS scan. The maximum injection time was set to 100 ms for MS and 50 ms for MS/MS. The isolation window for MS2 was set to 2 m/z and the normalized collision energy (stepped) was set as 27, 29 and 32 for fragmentation. Blank samples (75% ACN in water) and QC samples were injected every six samples during acquisition.

8.3 Bioinformatics analysis

(a) Data preprocessing and filtering

The raw MS data were processed using MS-DIAL for peak alignment, retention time correction and peak area extraction. The metabolites were identified by accuracy mass

(mass tolerance < 0.01 Da) and MS/MS data (mass tolerance < 0.02 Da), which were matched with HMDB and other public databases and our self-built metabolite standard library. In the extracted-ion features, only the variables having more than 50% of the nonzero measurement values in at least one group were kept.

(b) Multivariate statistical analysis

R(version:4.0.3) and R packages were used for all multivariate data analyses and modelling. Data were mean-centred using Pareto scaling. Models were built on principal component analysis (PCA) and orthogonal partial least-square discriminant analysis (OPLS-DA). All the models evaluated were tested for overfitting with methods of permutation tests (n = 200). OPLS-DA allowed the determination of discriminating metabolites using the variable importance on projection (VIP). The VIP score value indicates the contribution of a variable to the discrimination between all the classes of samples. Mathematically, these scores are calculated for each variable as a weighted sum of squares of PLS weights. The VIP values over 1 are considered significant. A high score is in agreement with a strong discriminatory ability and thus constitutes a criterion for the selection of biomarkers.

The p value was calculated by one-way analysis of variance (ANOVA) for multiple group analysis. Metabolites with VIP values greater than 1.0 and p values less than 0.05 were considered to be statistically significant metabolites. Fold change was calculated as the logarithm of the average mass response (area) ratio between two arbitrary classes. On the other hand, the identified differential metabolites were used to perform cluster analyses with the R package.

(c) KEGG enrichment analysis

To identify the perturbed biological pathways, the differential metabolite data were subjected to KEGG pathway analysis using KEGG database (http://www.kegg.jp). KEGG enrichment analyses were carried out with Fisher's exact test, and FDR correction for multiple testing was performed. Enriched KEGG pathways were nominally statistically significant at the $p<0.05$ level.

9. Statistics

All data are reported as the mean ± SD for the independent experiments. The unpaired two-tailed Student t-test was used for comparison between two groups, and ANOVAs were used for multi-component comparisons. $p< 0.05$ was considered statistically significant. Curve fitting was performed using GraphPad Prism 5 software.

Results

1. Effects of knockout of *Aqp9* on body weight

As shown in Figure 1, by the end of week 12, the body weight in each group of mice was measured. The weight at the end of the experiment remarkably differed. Compared with those of the WT-Control group, the weight of mice in the KO-Control group was significantly lower after 12 weeks ($p<0.01$). After 12 weeks of the experiment, compared with the WT-Control group, the WT-HFD group exhibited a significantly higher body weight ($p<0.01$). In contrast, knockout of *Aqp9* significantly decreased the body weight ($p < 0.01$) in the NAFLD mouse model.

2. Effects of knockout of *Aqp9* on serum index

To evaluate the therapeutic effects of knockout of *Aqp9*, we compared the levels of ALT, AST, TG, TC, HDL-C, and LDL-C in serum among the four groups. As shown in Figure 2, the serum levels of ALT, AST, TG, TC and LDL-C in the WT-HFD group were significantly higher and HDL-C lower than those in the WT-Control group (ALT, AST, and TC, $p<0.05$; TG, LDL-C, and HDL-C, $p<0.01$). However, compared with the WT-HFD, the biochemical serum parameters in the KO-HFD decreased significantly, other than HDL-C.

3. Antioxidative and anti-inflammatory effects of knockout of *Aqp9*

Previous studies have shown that knockout of *Aqp9* can suppress oxidative stress and inflammation, which play an important role in the progression of NAFLD. Thus, we further investigated whether knockout of *Aqp9* inhibited oxidative stress and inflammation in NAFLD mice. The results showed that the activities of SOD and GSH-Px were lower and the level of MDA was higher in the WT-HFD group than in the WT-Control group (SOD, and GSH-Px, $p<0.01$; MDA, $p<0.05$, Figure 3A, B,C). GSH-Px and SOD were increased, while the level of MDA was decreased in the KO-HFD group compared to those of the WT-HFD group (Figure 3A, B, C).

The levels of IL-6, IL-1β, and TNF-α in the liver tissue were higher in the WT-HFD group than in the WT-Control group ($p<0.01$, respectively, Figure 3D, E, F). Knockout of Aqp9 resulted in decreased levels of inflammatory factors compared to those in the WT-HFD group (Figure 3 D, E, F).

4. Effects of knockout of *Aqp9* on liver morphology

As shown in Figure 4, the liver samples in the HFD groups revealed varying degrees of fat infiltration and hepatomegaly. These changes were more prominent in the WT-HFD group than in the KO-HFD group. Although sections of lobular structures in the liver cells were unclear, the livers in the four groups revealed less fatty degeneration of liver cells and small lipid droplets. In the WT-HFD group, some lipid

droplets aggregated, resulting in slight steatosis. In the KO-HFD group, only partial reticular vacuolar degeneration appeared, but no obvious lipid droplets appeared. ORO staining showed red lipid droplets in the WT-HFD group, but decreased red lipid droplets in the KO-HFD group, indicating that knockout of *Aqp9* can effectively alleviate the progression of fatty liver, but can cause vacuolar degeneration. Moreover, knockout of *Aqp9* turned macrovesicular steatosis into microvesicular steatosis, and reduced the steatosis scale. Based on this evidence, we believe that knockout of *Aqp9* can improve hepatic steatosis in a HFD-induced mouse model.

5.Metabonomic profile analysis

5.1 Quality control

PCA is a statistical method that converts a set of possible related variables into a linear uncorrelated variable that can reveal the internal structure of the data to better interpret the variables. As shown in Figure 5A and B, PCA showed a clear group separation between the four groups and the distribution of QC samples converged. The OPLS-DA models indicated significant metabolic variations between the WT-Control group and the WT-HFD group (Figure 5C) as well as between the WT-HFD group and the KO-HFD group (Figure 5E). Likewise, seven- rounds of cross validation and 200 rounds of RPT showed that the OPLS-DA models were robust. Comparing the WT-HFD group with the WT-Control group, the R2 and Q2 values in the OPLS-DA model were 0.847 and 0.949, respectively (Figure 5D). Comparing the WT-HFD group with the KO-HFD group, the R^2 and Q^2 values in the OPLS-DA model were 0.825 and 0.95, respectively (Figure 5F).

5.2 Metabolic alterations between the WT-Control and WT-HFD groups

A total of 220 metabolites in the liver between the WT-Control and WT-HFD groups were detected via untargeted metabolomics, which were identified through filtering with the screening condition of $p < 0.05$ and VIP > 1 (Figure 6A, Table S1). Hierarchical clustering analysis of the differential metabolites helped to classify metabolites with the same characteristics into one class and find the characteristics of metabolites. Figure 6B shows that fatty acids and lipids were the differential metabolites classified by KEGG, which indicates the successful modelling of NAFLD. Metabolic pathway enrichment analysis was performed by the KEGG database to investigate the metabolic mechanism of differential metabolites that were affected by HFD feeding. The pathway analysis showed highly affected pathways, and the top 30 pathways are listed with the number of metabolites in Figure 6C. Glycerophospholipid metabolism and cholesterol metabolism were related to the development of NAFLD. The graph of the differential abundance score showed that

metabolites related to glycerophospholipid metabolism were increased in the WT-HFD group (Figure 6D).

5.3 Metabolic alterations between the KO-HFD and WT-HFD groups

Overall, 209 differential metabolites between the KO-HFD group and the WT-HFD group were identified (VIP>1 and $p<0.05$, Figure 7A, Table S2). The cluster analysis of the top 50 metabolites showed that the nine (18%) metabolites related to lipids, fatty lipids, and sterol lipids significantly changed (Figure 7B). The pathway analysis showed that fatty acid biosynthesis was significantly changed by knockout of *Aqp9* with HFD (Figure 7C), which included five metabolites. The specific differential metabolites for lipid metabolism are shown in Figure 7D. Four lipids decreased significantly, while one lipid precursor increased, as shown in Figure 7D. The interactions of pathways confirmed that metabolites related to the metabolism, elongation, degradation, and biosynthesis of fatty acids were connected with each other (Figure 7E). The Circos and Sankey graphs showed that most different metabolites were related to fatty acid metabolism (Figure 7F, G), suggesting that AQP9 has a vital role in fatty metabolism in NAFLD.

5.4 Metabolic alterations between KO-HFD, WT-HFD, and WT-Control groups

A total of 190 differential metabolites were observed among the three groups tested by one-way ANOVA. Lipids were also the prominent classification in the top 50 differential metabolites according to VIP value (Figure 8A, Table S3). The OPLS-DA models indicated significant metabolic variations among the three groups (Figure 8B), and the R^2 and Q^2 values in the OPLS-DA model were 0.994 and 0.773, respectively (Figure 8C). By the method of key means, 122 metabolites related to NAFLD were affected by knockout of *Aqp9* (Figure 8D). The enriched pathways by the metabolites also included important pathways in developing NAFLD, such as fatty acid biosynthesis, biosynthesis of unsaturated fatty acids, insulin signalling and glucagon signalling (Figure 8E).

Discussion

NAFLD, as a main hepatic manifestation of metabolic syndrome, represents a wide spectrum of histopathological abnormalities ranging from simple steatosis to nonalcoholic steatohepatitis (NASH) with or without fibrosis and, eventually, cirrhosis and hepatocellular carcinoma[19]. The mechanism of NAFLD is particularly complicated, involving the interplay between genetics and environmental factors and differing pathways [6, 20]. Emerging evidence has proven that AQP9 is involved in

lipid-lowering activity and could be a novel target for NAFLD[11, 15, 21, 22]. In the present study, we first explored the role of AQP9 in NAFLD by untargeted metabolomics through knockout of *Aqp9*.

Before investigating metabolic alterations, we measured physiological changes, such as body weight and serum index. Interestingly, the KO-Control group showed significantly lower body weight than did the WT-Control group. Knockout of *Aqp9* affected mouse body weight, which could be explained by defective glycerol metabolism in *Aqp9*$^{-/-}$ mice[23]. It was apparent that the KO-HFD group had less weight gain than did the WT-HFD group, which proved that *Aqp9*$^{-/-}$ mice had good tolerance to a HFD. We reported that LDL-C, TC, TG, ALT, and AST in serum were significantly increased and that HDL-C was decreased after HFD modelling. This finding was consistent with a previous NAFLD model[24]. After knockout of *Aqp9*, the lipid index in the serum did not change significantly after HFD feeding, which suggested that *Aqp9* knockout could antagonize the accumulation of lipids in the serum.

Chronic inflammation is also an important factor in promoting the progression of NASH to the development of NAFLD[25]. Classic inflammation related factors, such as IL-6, IL-10, and TNF-*α*, were selected for ELISA verification. They were significantly increased after modelling, while the level in the KO-HFD group was increased less than that in the WT-HFD group after modelling. This result suggested that NAFLD could induce an inflammatory response and that knockout of *Aqp9* can antagonize this inflammatory response. The overproduction of reactive oxygen species and consequent oxidative stress contribute to the pathogenesis of NAFLD[26]. It is now acknowledged that impaired lipid metabolism and oxidative stress have a close relationship[27]. SOD, CAT, and GSH-PX are three major antioxidant enzymes that reflect the antioxidant capacity of tissues. After modelling, the enzyme activities decreased, while the KO-HFD group showed a decreasing trend compared with that in the WT-HFD group. Knockout of *Aqp9* antagonized this oxidative stress injury to improve the capacity of antioxidant defence systems. The results confirmed that serum lipids, inflammation, and oxidative stress play vital roles in the development of NAFLD and that knockout of *Aqp9* could antagonize the progression of NAFLD.

In the study, we mainly tested serological markers reflecting liver function and blood lipids levels. There were statistically significant changes after the modelling. However, the liver morphology showed only mild steatosis. Compared with liver morphology, the changes of serological indexes were more obvious. We speculate that the change of serological indexes is earlier than that of liver histomorphology. In addition, serological indexes are quantitative analysis after biochemical testing. Compared with

morphology, it has quantifiable indexes, so the changes of serological indexes are more significant. In addition, the modelling method in this study was that mice received a HFD for 12 weeks, and the liver pathology was still in the early stage of steatosis. Morphological observation showed only mild hepatocyte steatosis. Although lipid droplets are formed, they have not yet developed into diffuse aggregation. Thuy T.P. Nguyen et al.[28] showed diffuse accumulation of lipid droplets in the liver, although the model was also fed for 12 weeks. We suspect that the difference is due to the experimental environment. To avoid fighting among mice, we kept only one mouse in each cage, which may reduce their food intake and delay the progression of NAFLD. However, all mice in this experiment were in the same environment, and the experimental variables were strictly controlled. The purpose of our experiment is to observe the role of AQP9 in the early pathogenesis of NAFLD and its influence on metabolism, so the mild steatosis formed in this experiment is more consistent with this study.

Based on integrative pathway analysis, we focused on a pathway named fatty acid biosynthesis for development. NAFLD results from imbalanced lipid homeostasis in the liver. In the present study, six biomarkers related to fatty acid metabolism changed in the NAFLD model, which proved the successful establishment of the NAFLD model. The levels of palmitic acid, stearic acid, deconaic acid, and myristic acid were reduced, indicating that fatty acid metabolism was inhibited, while the acetyl coenzyme A was elevated. Free fatty acids are the major mediators of hepatic steatosis and correlate with disease severity[29, 30]. The results of our study first proved that knockout of *Aqp9* could induce fewer fatty acids in the liver thus protecting mice from NAFLD. Previous studies showed that knockdown of AQP9 could reduce the accumulation of TG in hepatocytes in a model for NAFLD, but the exact mechanism was not shown. In our present study, acetyl coenzyme A was lower in the KO-HFD groups than in the WT-HFD groups, which could be explained by *Aqp9* being a target gene of PPARα, which is involved in fatty acid oxidation[31]. Knockout of Aqp9 could lead to negative feedback of stimulation for PPARα[32]. Elevated fatty acid oxidation is a mechanism to decrease fatty acids, thus increasing the acetyl coenzyme A. In conclusion, we first identified AQP9 as being involved in downregulating fatty acid biosynthesis to antagonize the development of NAFLD.

Moreover, insulin resistance (IR) is also a key factor in the pathogenesis and potential evolution of hepatic steatosis[33, 34]. IR in adipose tissue results in increased lipolysis in adipocytes and an increase in circulating FFA, which further exacerbates steatosis and IR in muscle tissue. The higher acetyl coenzyme A in *Aqp9*$^{-/-}$ mice could induce less insulin resistance and antagonize the development of NAFLD. The higher adenosine 3',5'- cyclic monophosphate in *Aqp9*$^{-/-}$ can directly stimulate insulin

secretion. Thus, knockout of *Aqp9* may play an important role against insulin resistance results in defective hepatic glycerol metabolism due to lower intrahepatocellular glycerol levels.

Our previous study[14] found that AQP9 could be used as an intervention target to antagonize the occurrence of early chronic liver injury. Knockout of *Aqp9* gene can affect downstream inflammation, oxidative stress, apoptosis and pyroptosis by reducing hepatic lipotoxicity. In this study, we also found that knockout of *Aqp9* could resist HFD-induced inflammation and oxidative stress. Inflammation and oxidative stress in NAFLD are mainly caused by lipid peroxidation, and this study also found that AQP9 mainly affected lipid metabolism in NAFLD. Knockout of *Aqp9* can reduce lipid toxicity, and then reducing downstream inflammation and oxidative stress.

Adipose tissue, liver and small intestine are the main sites for TG synthesis in the body, among which liver has the strongest synthesis ability. The triglyceride (TG) synthesized in the liver is combined with apolipoprotein, phospholipid and cholesterol to form very low density lipoprotein cholesterol (VLDL-C), which is secreted into the blood by hepatocytes and transported to extrahepatic tissues. If the amount of TG synthesized in the liver exceeds the upper limit of VLDL-C production, or the liver is unable to produce VLDL-C to secret it into the blood, it will accumulate in hepatocytes, resulting in steatosis of hepatocytes and fatty liver[35]. Fat mobilization and transport are closely related to AQPs, especially AQP7 and AQP3 in adipocytes and AQP9 in liver tissue[36]. AQP7 in adipocytes transports glycerol from adipose tissue to the blood for transport to the liver. Glycerol is then taken up by AQP9 in hepatocytes. These two AQPs coordinate the transport of glycerol from adipose tissue to the liver[22]. The abnormal expression of AQP9 in hepatocytes can lead to the imbalance of intracellular and extracellular glycerol, and then cause the disorder of lipid metabolism, leading to the accumulation of TG in hepatocytes. For example, increased AQP9 expression would cause a large amount of glycerol to enter hepatocytes, exceeding the compensatory capacity of the liver, thus leading to increased hepatic TG synthesis and intracellular accumulation. In this study, *Aqp9*$^{-/-}$ mice were used to confirm that *Aqp9* knockout can effectively alleviate hepatocyte steatosis and resist the progression of NAFLD.

Despite such findings, our study has some limitations. First, the number of mice used in this study was six per group; hence, the performance of our statistical analysis needs to be validated in a large study. Second, for the investigation of the role of AQP9, knockout *Aqp9* mouse was constructed, which had a great impact on the mouse lifespan. This method cannot be applied in the clinical setting, but it is hopeful

in the study of the mechanism of NAFLD. Third, a model of NAFLD was established by HFD, which could lead to heterogeneous NAFLD due to fatty resistance. Lastly, most of the mice were in the early stages of NAFLD and they were not able to represent the various stages of NAFLD.

Conclusion

In conclusion, in this study, we first examined the role of AQP9 in NAFLD by constructing *Aqp9*$^{-/-}$ mice and an NAFLD model. We demonstrated that knockout of *Aqp9* could antagonize the development of NAFLD by reducing inflammation and oxidative stress. Untargeted metabolomic analysis indicated that fatty acid biosynthesis and insulin resistance were important pathways that knockout of *Aqp9* could influence. Our findings provide evidence of the potential therapeutic effectiveness of AQP9 in NAFLD. Further studies are required to clarify the molecular mechanisms of action of AQP9 in lipid accumulation in NAFLD.

Author contributions

Q.C., J.Z., W.Z, X.L, Y.X. designed the study; Q.C., J.Z., J.F. and H.D. carried out experiments; Q.C., J.Z., and H.D. analyzed the data; J.F. and H.D. made the figures; Q.C., J.W., and W.Z. drafted and revised the paper; all authors approved the final version of the manuscript.

Declaration of competing interest

The authors declare that they have no known competing financial interests or personal relationships that could have appeared to influence the work reported in this paper.

Availability of data and materials

The datasets used and/or analyzed during the current study are included in this article and its supplementary information files. The datasets are available from the corresponding author on reasonable request.

Acknowledgments

We thank Jiye Hou at Shanghai Bioprofile Technology Company Ltd. for his technical support in proteomics.

Funding

This work was supported by the CAMS Innovation Fund for Medical Sciences (CIFMS) (No. 2020-I2M-CT-B-026).

References:

1 Zhou J, Zhou F, Wang W, et al. Epidemiological Features of NAFLD From 1999 to 2018 in China. *Hepatology* 2020; **71**(5): 1851-1864; [DOI: 10.1002/hep.31150]

2 Younossi Z, Anstee QM, Marietti M, et al. Global burden of NAFLD and NASH: trends, predictions, risk factors and prevention. *Nat Rev Gastroenterol Hepatol* 2018; **15**(1): 11-20; [DOI: 10.1038/nrgastro.2017.109]

3 Byrne CD, Targher G. NAFLD: a multisystem disease. *J Hepatol* 2015; **62**(1 Suppl): S47-64; [DOI: 10.1016/j.jhep.2014.12.012]

4 Targher G, Byrne CD, Tilg H. NAFLD and increased risk of cardiovascular disease: clinical associations, pathophysiological mechanisms and pharmacological implications. *Gut* 2020; **69**(9): 1691-1705; [DOI: 10.1136/gutjnl-2020-320622]

5 Ferguson D, Finck BN. Emerging therapeutic approaches for the treatment of NAFLD and type 2 diabetes mellitus. *Nat Rev Endocrinol* 2021; **17**(8): 484-495; [DOI: 10.1038/s41574-021-00507-z]

6 Friedman SL, Neuschwander-Tetri BA, Rinella M, et al. Mechanisms of NAFLD development and therapeutic strategies. *Nat Med* 2018; **24**(7): 908-922; [DOI: 10.1038/s41591-018-0104-9]

7 Huebert RC, Splinter PL, Garcia F, et al. Expression and localization of aquaporin water channels in rat hepatocytes. Evidence for a role in canalicular bile secretion. *J Biol Chem* 2002; **277**(25): 22710-22717; [DOI: 10.1074/jbc.M202394200]

8 Calamita G, Ferri D, Gena P, et al. Altered expression and distribution of aquaporin-9 in the liver of rat with obstructive extrahepatic cholestasis. *Am J Physiol Gastrointest Liver Physiol* 2008; **295**(4): G682-690; [DOI: 10.1152/ajpgi.90226.2008]

9 Xiang T, Ge S, Wen J, et al. The possible association between AQP9 in the intestinal epithelium and acute liver injury-induced intestinal epithelium damage. *Mol Med Rep* 2018; **18**(6): 4987-4993; [DOI: 10.3892/mmr.2018.9542]

10 Carbrey JM, Gorelick-Feldman DA, Kozono D, et al. Aquaglyceroporin AQP9: solute permeation and metabolic control of expression in liver. *Proc Natl Acad Sci U S A* 2003; **100**(5): 2945-2950; [DOI: 10.1073/pnas.0437994100]

11 Gena P, Mastrodonato M, Portincasa P, et al. Liver glycerol permeability and aquaporin-9 are dysregulated in a murine model of Non-Alcoholic Fatty Liver Disease. *PLoS One* 2013; **8**(10): e78139; [DOI: 10.1371/journal.pone.0078139]

12 Cai C, Wang C, Ji W, et al. Knockdown of hepatic aquaglyceroporin-9 alleviates high fat diet-induced non-alcoholic fatty liver disease in rats. *Int Immunopharmacol*

2013; **15**(3): 550-556; [DOI: 10.1016/j.intimp.2013.01.020]

13 Wang C, Lv ZL, Kang YJ, et al. Aquaporin-9 downregulation prevents steatosis in oleic acid-induced non-alcoholic fatty liver disease cell models. *Int J Mol Med* 2013; **32**(5): 1159-1165; [DOI: 10.3892/ijmm.2013.1502]

14 Cheng Q, Ding H, Fang J, et al. Aquaporin 9 Represents a Novel Target of Chronic Liver Injury That May Antagonize Its Progression by Reducing Lipotoxicity. *Oxid Med Cell Longev* 2021; **2021**: 5653700; [DOI: 10.1155/2021/5653700]

15 Baldini F, Portincasa P, Grasselli E, et al. Aquaporin-9 is involved in the lipid-lowering activity of the nutraceutical silybin on hepatocytes through modulation of autophagy and lipid droplets composition. *Biochim Biophys Acta Mol Cell Biol Lipids* 2020; **1865**(3): 158586; [DOI: 10.1016/j.bbalip.2019.158586]

16 Johnson CH, Ivanisevic J, Siuzdak G. Metabolomics: beyond biomarkers and towards mechanisms. *Nat Rev Mol Cell Biol* 2016; **17**(7): 451-459; [DOI: 10.1038/nrm.2016.25]

17 Piras C, Noto A, Ibba L, et al. Contribution of Metabolomics to the Understanding of NAFLD and NASH Syndromes: A Systematic Review. *Metabolites* 2021; **11**(10); [DOI: 10.3390/metabo11100694]

18 Masoodi M, Gastaldelli A, Hyötyläinen T, et al. Metabolomics and lipidomics in NAFLD: biomarkers and non-invasive diagnostic tests. *Nat Rev Gastroenterol Hepatol* 2021; **18**(12): 835-856; [DOI: 10.1038/s41575-021-00502-9]

19 Eslam M, Valenti L, Romeo S. Genetics and epigenetics of NAFLD and NASH: Clinical impact. *J Hepatol* 2018; **68**(2): 268-279; [DOI: 10.1016/j.jhep.2017.09.003]

20 Bessone F, Razori MV, Roma MG. Molecular pathways of nonalcoholic fatty liver disease development and progression. *Cell Mol Life Sci* 2019; **76**(1): 99-128; [DOI: 10.1007/s00018-018-2947-0]

21 Badaut J, Regli L. Distribution and possible roles of aquaporin 9 in the brain. *Neuroscience* 2004; **129**(4): 971-981; [DOI: 10.1016/j.neuroscience.2004.06.035]

22 Lebeck J. Metabolic impact of the glycerol channels AQP7 and AQP9 in adipose tissue and liver. *J Mol Endocrinol* 2014; **52**(2): R165-178; [DOI: 10.1530/JME-13-0268]

23 Rojek AM, Skowronski MT, Füchtbauer EM, et al. Defective glycerol metabolism in aquaporin 9 (AQP9) knockout mice. *Proc Natl Acad Sci U S A* 2007; **104**(9): 3609-3614; [DOI: 10.1073/pnas.0610894104]

24 Van Herck MA, Vonghia L, Francque SM. Animal Models of Nonalcoholic Fatty Liver Disease-A Starter's Guide. *Nutrients* 2017; **9**(10); [DOI: 10.3390/nu9101072]

25 Schuster S, Cabrera D, Arrese M, et al. Triggering and resolution of inflammation in NASH. *Nat Rev Gastroenterol Hepatol* 2018; **15**(6): 349-364; [DOI: 10.1038/s41575-018-0009-6]

26 Hong T, Chen Y, Li X, et al. The Role and Mechanism of Oxidative Stress and

Nuclear Receptors in the Development of NAFLD. *Oxid Med Cell Longev* 2021; **2021**: 6889533; [DOI: 10.1155/2021/6889533]

27 Arroyave-Ospina JC, Wu Z, Geng Y, et al. Role of Oxidative Stress in the Pathogenesis of Non-Alcoholic Fatty Liver Disease: Implications for Prevention and Therapy. *Antioxidants (Basel)* 2021; **10**(2); [DOI: 10.3390/antiox10020174]

28 Nguyen TTP, Kim DY, Lee YG, et al. SREBP-1c impairs ULK1 sulfhydration-mediated autophagic flux to promote hepatic steatosis in high-fat-diet-fed mice. *Mol Cell* 2021; **81**(18): 3820-3832 e3827; [DOI: 10.1016/j.molcel.2021.06.003]

29 Park HS, Song JW, Park JH, et al. TXNIP/VDUP1 attenuates steatohepatitis via autophagy and fatty acid oxidation. *Autophagy* 2021; **17**(9): 2549-2564; [DOI: 10.1080/15548627.2020.1834711]

30 Marra F, Svegliati-Baroni G. Lipotoxicity and the gut-liver axis in NASH pathogenesis. *J Hepatol* 2018; **68**(2): 280-295; [DOI: 10.1016/j.jhep.2017.11.014]

31 Jiang YJ, Kim P, Lu YF, et al. PPARgamma activators stimulate aquaporin 3 expression in keratinocytes/epidermis. *Exp Dermatol* 2011; **20**(7): 595-599; [DOI: 10.1111/j.1600-0625.2011.01269.x]

32 Lebeck J, Cheema MU, Skowronski MT, et al. Hepatic AQP9 expression in male rats is reduced in response to PPARα agonist treatment. *Am J Physiol Gastrointest Liver Physiol* 2015; **308**(3): G198-205; [DOI: 10.1152/ajpgi.00407.2013]

33 Fujii H, Kawada N, Japan Study Group Of Nafld J-N. The Role of Insulin Resistance and Diabetes in Nonalcoholic Fatty Liver Disease. *Int J Mol Sci* 2020; **21**(11); [DOI: 10.3390/ijms21113863]

34 Tanase DM, Gosav EM, Costea CF, et al. The Intricate Relationship between Type 2 Diabetes Mellitus (T2DM), Insulin Resistance (IR), and Nonalcoholic Fatty Liver Disease (NAFLD). *J Diabetes Res* 2020; **2020**: 3920196; [DOI: 10.1155/2020/3920196]

35 Semova I, Biddinger SB. Triglycerides in Nonalcoholic Fatty Liver Disease: Guilty Until Proven Innocent. *Trends Pharmacol Sci* 2021; **42**(3): 183-190; [DOI: 10.1016/j.tips.2020.12.001]

36 Rodriguez A, Moreno NR, Balaguer I, et al. Leptin administration restores the altered adipose and hepatic expression of aquaglyceroporins improving the non-alcoholic fatty liver of ob/ob mice. *Sci Rep* 2015; **5**: 12067; [DOI: 10.1038/srep12067]

Graphical abstract

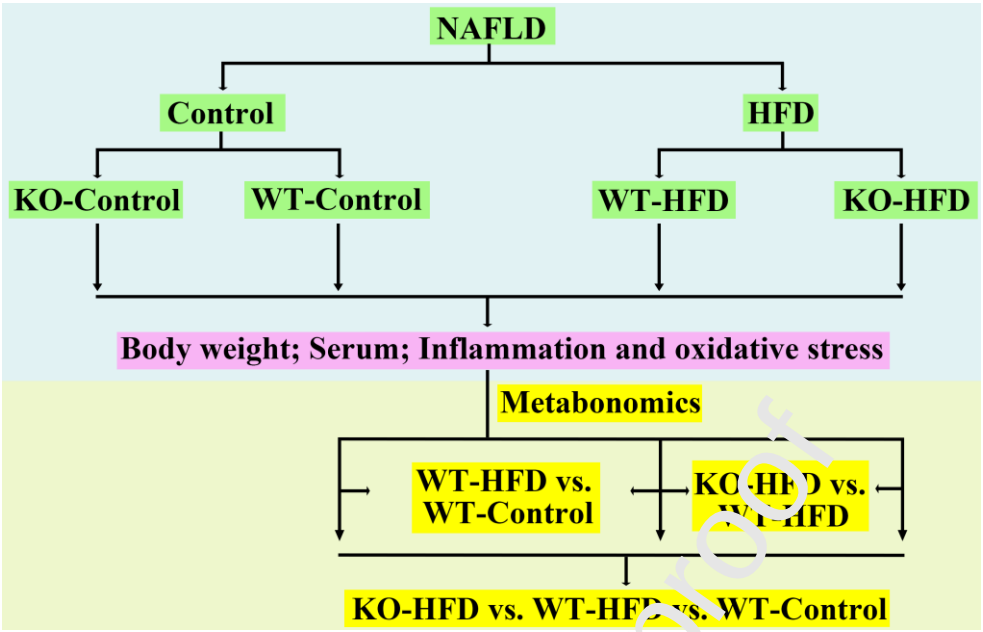

Highlights:

Knockout of *Aqp9* can antagonize the development of NAFLD.

Knockout of *Aqp9* can reduce inflammation and oxidative stress.

Fatty acid biosynthesis and insulin resistance are involved in AQP9-mediated NAFLD.

AQP9 is the potential therapeutic target of NAFLD.

Figure 1: Weight changes in the four groups. Weights at the end of the experiment remarkably differed. Compared with the WT-Control group, the weight in the KO-Control group was significantly lower after 12 weeks. Compared with the WT-Control group, the WT-HFD group exhibited a significantly higher weight. In contrast, knockout of *Aqp9* significantly decreased weight in the NAFLD mouse model. Data are mean ± s.e.m.; n=6. The two-way ANOVAs were used for statistical analysis followed by Tukey's multiple comparisons test. $^{**}p < 0.01$, compared with the WT-Control; ## $p<0.01$, compared with the WT-HFD.

Figure 2: Serum index among the four groups. (A-F) Statistical graphs of serum ALT, AST, TG, TC, LDL-C, and HDL-C, respectively. The serum levels of ALT, AST, TG, TC and LDL-C in the WT-HFD group were significantly higher and HDL-C lower than those in the WT-Control group. However, compared with the WT-HFD, the biochemical serum parameters in the KO-HFD decreased significantly, other than HDL-C. Data are mean ± s.e.m.; n=6. The one-way ANOVAs were used for statistical analysis followed by Bonferroni's post hoc test. $^{*}p<0.05$, $^{**}p<0.01$.

Figure 3: Oxidative stress and pro-inflammatory factors in the four groups. (A-C) Statistical graphs of liver tissue SOD, GSH-Px, and MDA, respectively. The activities of SOD and GSH-Px were lower and the level of MDA was higher in the WT-HFD group than in the WT-Control group. GSH-Px and SOD were increased, while the level of MDA was decreased in the KO-HFD group compared to those of the WT-HFD group. (D-F) Statistical graphs of liver tissue IL-6, IL-1β, and TNF-α respectively. The levels of IL-6, IL-1β, and TNF-α were higher in the WT-HFD group than in the WT-Control group. Knockout of Aqp9 resulted in decreased levels of inflammatory factors compared to those in the WT-HFD group. Data are mean ± s.e.m.; n=6. The one-way ANOVAs were used for statistical analysis followed by Bonferroni's post hoc test. $^{*}p<0.05$, $^{**}p<0.01$.

Figure 4: Lipid deposition occurring in the liver. The liver samples in the HFD groups revealed varying degrees of fat infiltration. These changes were more prominent in the WT-HFD group than in the KO-HFD group. In the WT-HFD group, some lipid droplets aggregated, resulting in slight steatosis. In the KO-HFD group, only partial reticular vacuolar degeneration appeared, but no obvious lipid droplets appeared. ORO staining showed red lipid droplets in the WT-HFD group, but decreased red lipid

droplets in the KO-HFD group, indicating that knockout of Aqp9 can effectively alleviate the progression of fatty liver, but can cause vacuolar degeneration. Moreover, knockout of *Aqp9* turned macrovesicular steatosis into microvesicular steatosis, and reduced the steatosis scale. The scale bar refers to 100 μm.

Figure 5: Quality control of the metabolomics data. (A, B) Score plots of PCA among the four groups. PCA showed a clear group separation between the four groups and the distribution of QC samples converged. (C, D) Score plots of OPLS-DA between the WT-Control group and the WT-HFD model group and the corresponding coefficient of loading plots. The OPLS-DA models indicated significant metabolic variations between the WT-Control group and the WT-HFD group. (E, F) Score plots of OPLS-DA between the KO-HFD group and the WT-HFD group and the corresponding coefficient of loading plots. The OPLS-DA models indicated significant metabolic variations between the KO-HFD group and the WT-HFD group.

Figure 6: Metabolic alterations between the WT-Control and WT-HFD groups. (A) Heatmap of different metabolites. (B) Classification of differential metabolites; we focused on FA Fatty acyls and lipids. (C) The KEGG analysis showed highly affected pathways; we have listed only the top 30 pathways with the number of metabolites; we focused on glycerophospholipid metabolism and cholesterol metabolism. (D) The graph of differential abundance scores showed that metabolites related to glycerophospholipid metabolism were increased in the WT-HFD group. The differential metabolites in glycerophospholipid metabolism include sn-glycero-3-phosphocholine, CDP-choline, phosphocholine, and acetylcholine. The differential metabolites in cholesterol metabolism include free cholesterol and bile acid.

Figure 7: Metabolic alterations between the KO-HFD and WT-HFD groups. (A) Heatmap of different metabolites. (B) Classification of differential metabolites. We focused on FA Fatty acyls, lipids, and ST sterol lipids. (C) The KEGG analysis showed highly affected pathways; we have listed only the top 30 pathways with the number of metabolites; we focused on fatty acid biosynthesis. The differential metabolites in fatty acid biosynthesis include palmitic acid, stearic acid, decanoic acid, myristic acid, and acetyl coenzyme A. (D) The specific differential metabolites for lipid metabolism. The four lipids decreased significantly, while one lipid precursor increased. Data are mean ± s.e.m.; n=6. The unpaired two-tailed Student t-test were used for statistical analysis. $*p<0.05$, $**p<0.01$. (E) The interactions of pathways confirmed that metabolites related to the metabolism, elongation, degradation, biosynthesis of fatty acid were connected with each other. (F) The Circos graph of the

KEGG pathway showed that most of the various metabolites were related to fatty acid metabolism. (G) The Sankey graph of KEGG pathway showed that most of the various metabolites were related to fatty acid metabolism.

Figure 8: Metabolic alterations among the KO-HFD, WT-HFD and WT-Control groups. (A) The complex heatmap of the top 50 different metabolites. (B, C) Score plots of OPLS-DA in the three groups and the corresponding coefficient of loading plots. The OPLS-DA models indicated significant metabolic variations among the three groups. (D) The changes in k-means in the three groups. 122 metabolites related to NAFLD were affected by knockout of Aqp9. (E) The most prominent KEGG pathways showed that most of the various metabolites were related to the fatty acid biosynthesis, biosynthesis of unsaturated fatty acids, insulin signaling pathway and glucagon signaling pathway. The differential metabolites in fatty acid biosynthesis include palmitic acid, stearic acid, decanoic acid, myristic acid, and acetyl coenzyme A. The differential metabolites in biosynthesis of unsaturated fatty acids include palmitic acid, stearic acid, and arachidic acid. cAMP is the only differential metabolite in insulin signaling pathway. The differential metabolites in glucagon signaling pathway include acetyl coenzyme A and cAMP.

Table 1 DNA extraction lysate formulation (pH = 7.4).

Solute	Concentration
Tris-HCl	0.1 mol/L
EDTA	5 mmol/L
NaCl	0.2 mol/L
SDS	0.2%
PK	10%

EDTA: ethylene diamine tetraacetic acid; SDS: sodium dodecyl sulfate; PK: protease K.

Table 2 The reaction procedure of PCR

Stage	Temperature (℃)	Time	Cycles
1	94	2 min	
2	98	10 s	
3	60	30 s	35
4	68	30 s	
5	68	10 min	
6	16	2 min	

Table 3 The reaction system of PCR

Component	Volume (μl)
ddH2O	9.5
2×Taq PCR Master	12.5
5'-primer (10 μmol/L)	1
3'-primer (10 μmol/L)	1

DNA template	1

Table 4: The primers of PCR

Purpose	Name	Sequence (5'~3')	Size (bp)
To detect *Aqp9* gene knockout	F	ATGCAGTAGCCACTTGTAGGC	KO：290
	R	ACCATATCCTGAGCTGGGCT	
To amplify the WT fragment of *Aqp9* gene	F	ATGCAGTAGCCACTTGTAGGC	WT：436
	WT-R	AGCAAGGGGCATTGTAAATC	

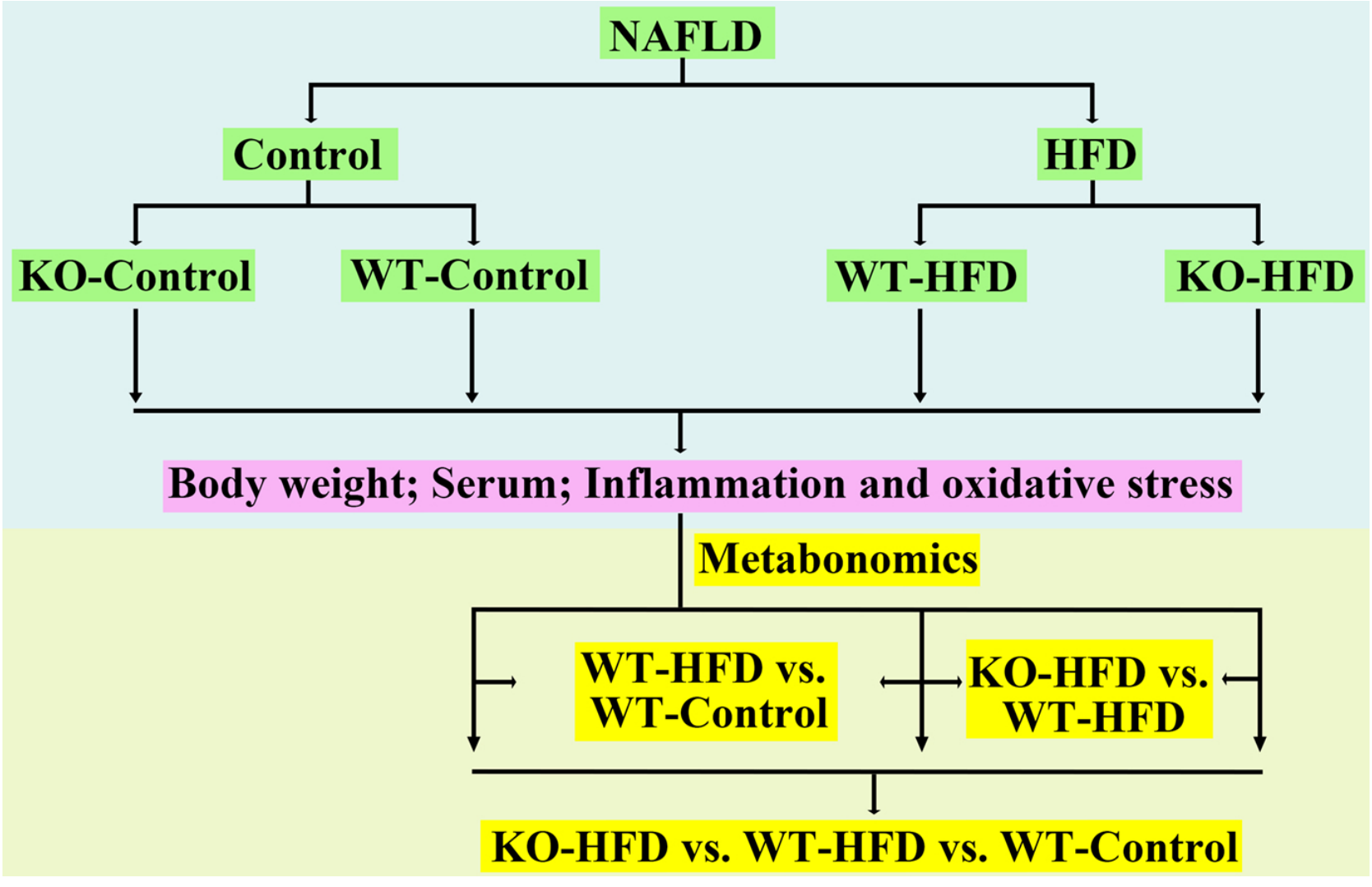

Graphics Abstract

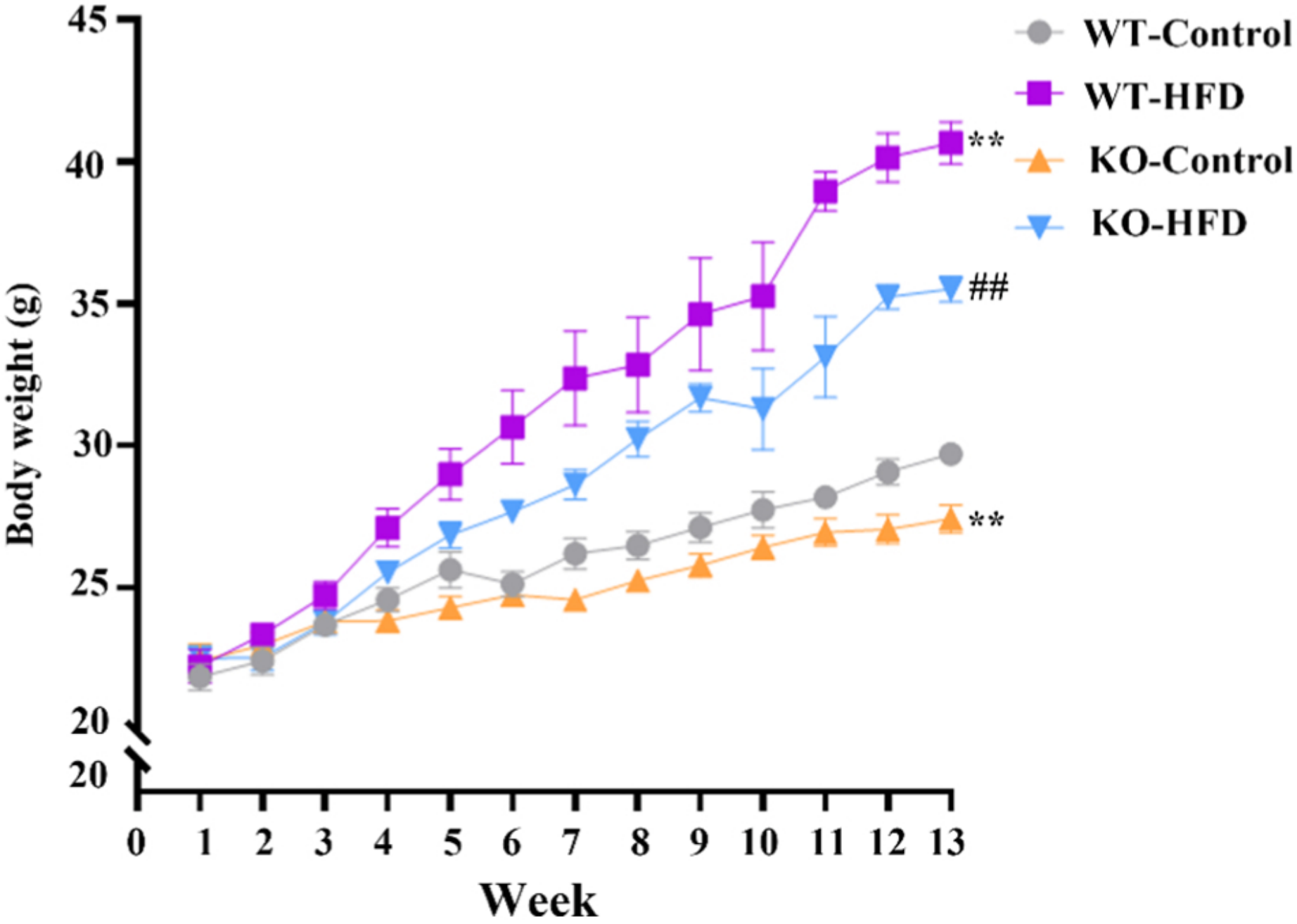
45
40
35
30
25
20
20
Body weight (g)
0
1
2
3
4
5
6
7
8
9
10
11
12
13
Week
WT-Control
WT-HFD
KO-Control
KO-HFD
**
##
**

Figure 1

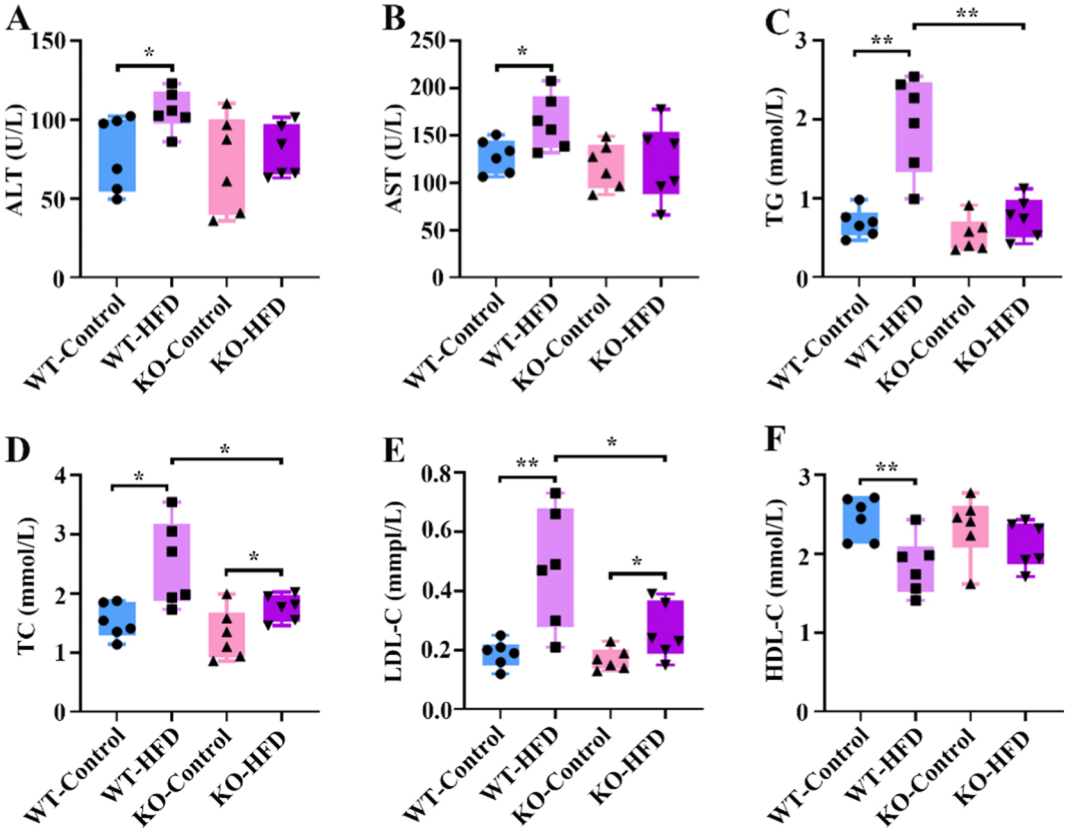
A
ALT (U/L)
150
100
50
0
*
B
AST (U/L)
250
200
150
100
50
0
*
C
TG (mmol/L)
3
2
1
0
**
**
D
TC (mmol/L)
4
3
2
1
0
*
*
E
LDL-C (mmpl/L)
0.8
0.6
0.4
0.2
0.0
**
*
F
HDL-C (mmol/L)
3
2
1
0
**
WT-Control
WT-HFD
KO-Control
KO-HFD

Figure 2

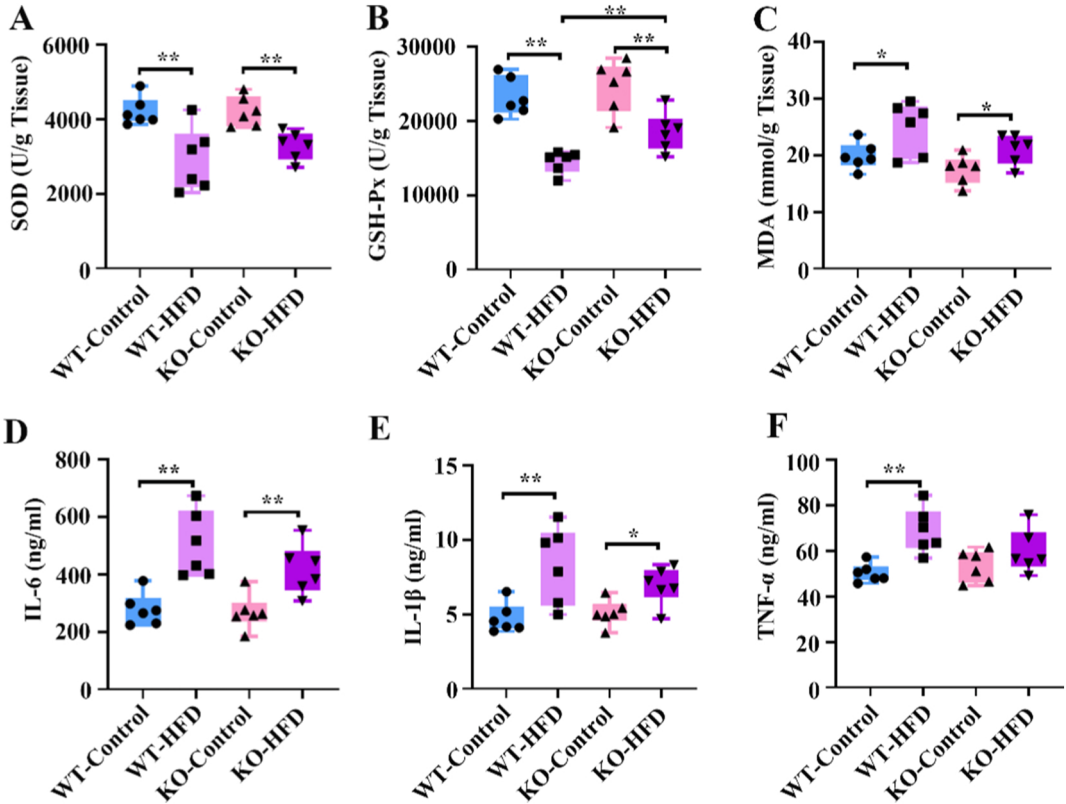
A
SOD (U/g Tissue)
6000
4000
2000
0
**
**
WT-Control
WT-HFD
KO-Control
KO-HFD
B
GSH-Px (U/g Tissue)
30000
20000
10000
0
**
**
**
C
MDA (mmol/g Tissue)
40
30
20
10
0
*
*
D
IL-6 (ng/ml)
800
600
400
200
0
**
**
E
IL-1β (ng/ml)
15
10
5
0
**
*
F
TNF-α (ng/ml)
100
80
60
40
20
0
**

Figure 3

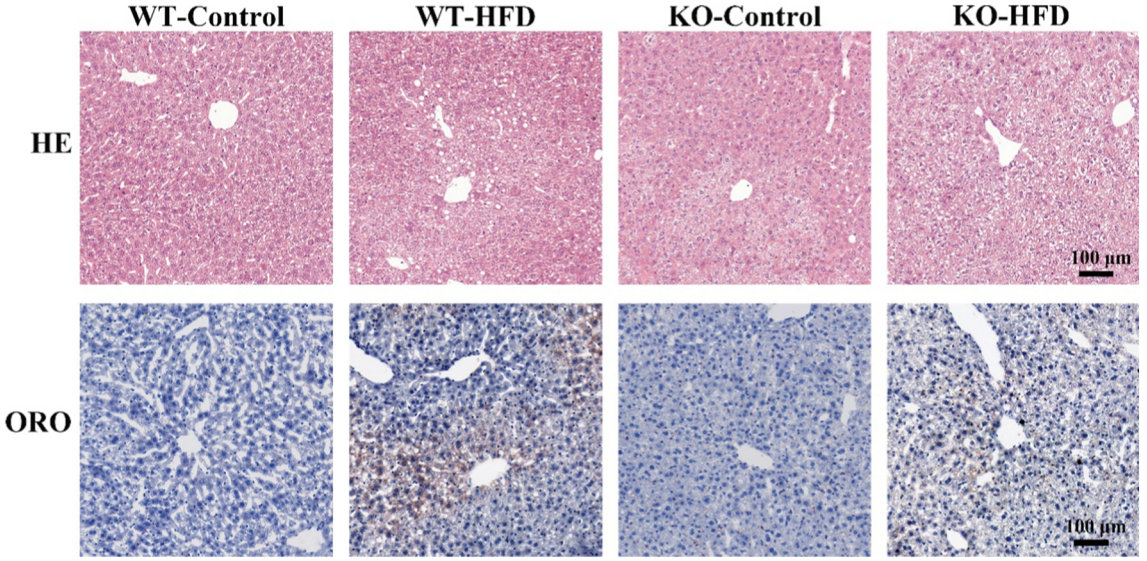

Figure 4

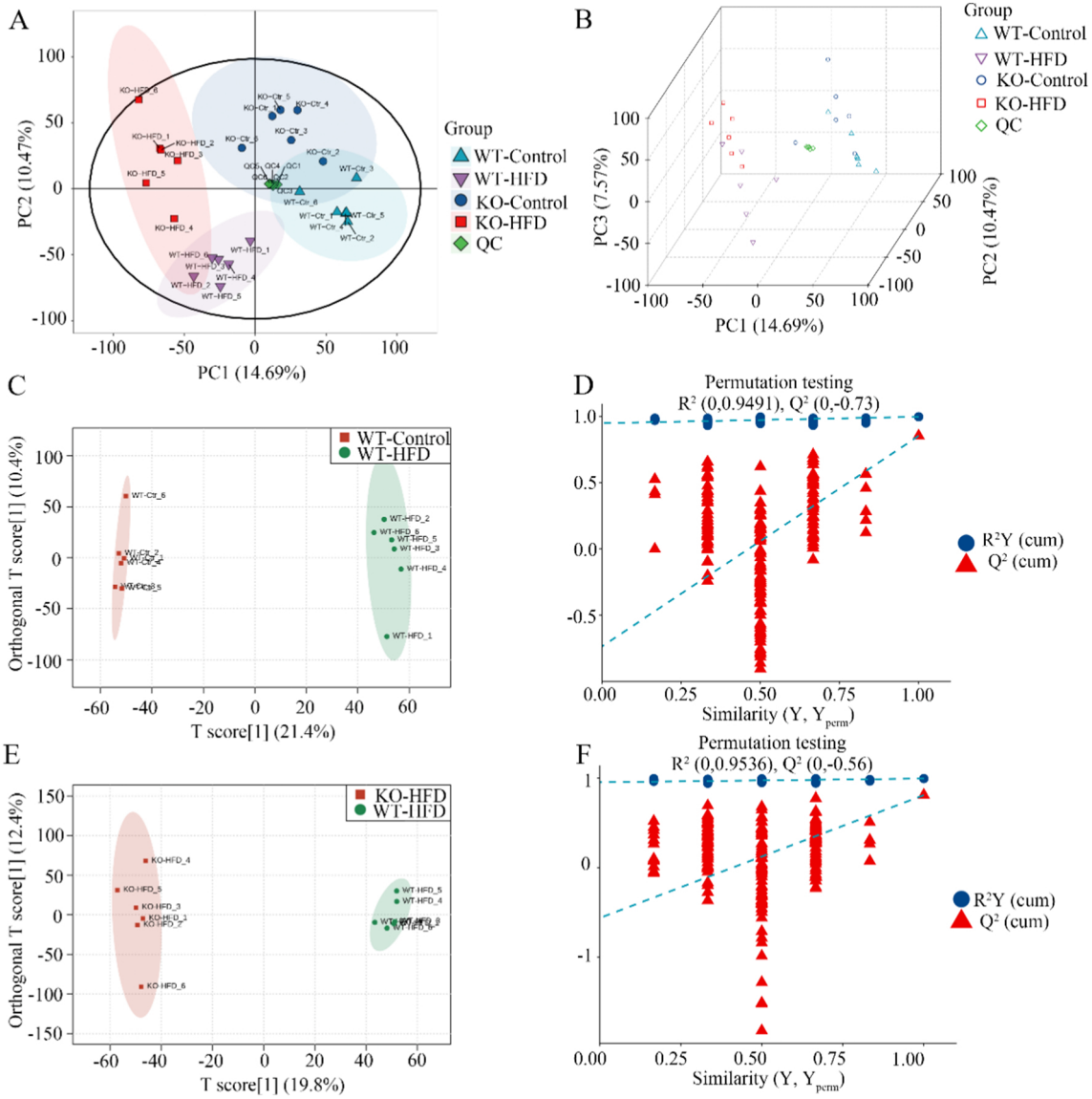
A
PC1 (14.69%)
PC2 (10.47%)
Group
WT-Control
WT-HFD
KO-Control
KO-HFD
QC
B
PC1 (14.69%)
PC2 (10.47%)
PC3 (7.57%)
Group
WT-Control
WT-HFD
KO-Control
KO-HFD
QC
C
WT-Control
WT-HFD
T score[1] (21.4%)
Orthogonal T score[1] (10.4%)
D
Permutation testing
R² (0,0.9491), Q² (0,-0.73)
R²Y (cum)
Q² (cum)
Similarity (Y, Y_perm)
E
KO-HFD
WT-HFD
T score[1] (19.8%)
Orthogonal T score[1] (12.4%)
F
Permutation testing
R² (0,0.9536), Q² (0,-0.56)
R²Y (cum)
Q² (cum)
Similarity (Y, Y_perm)

Figure 5

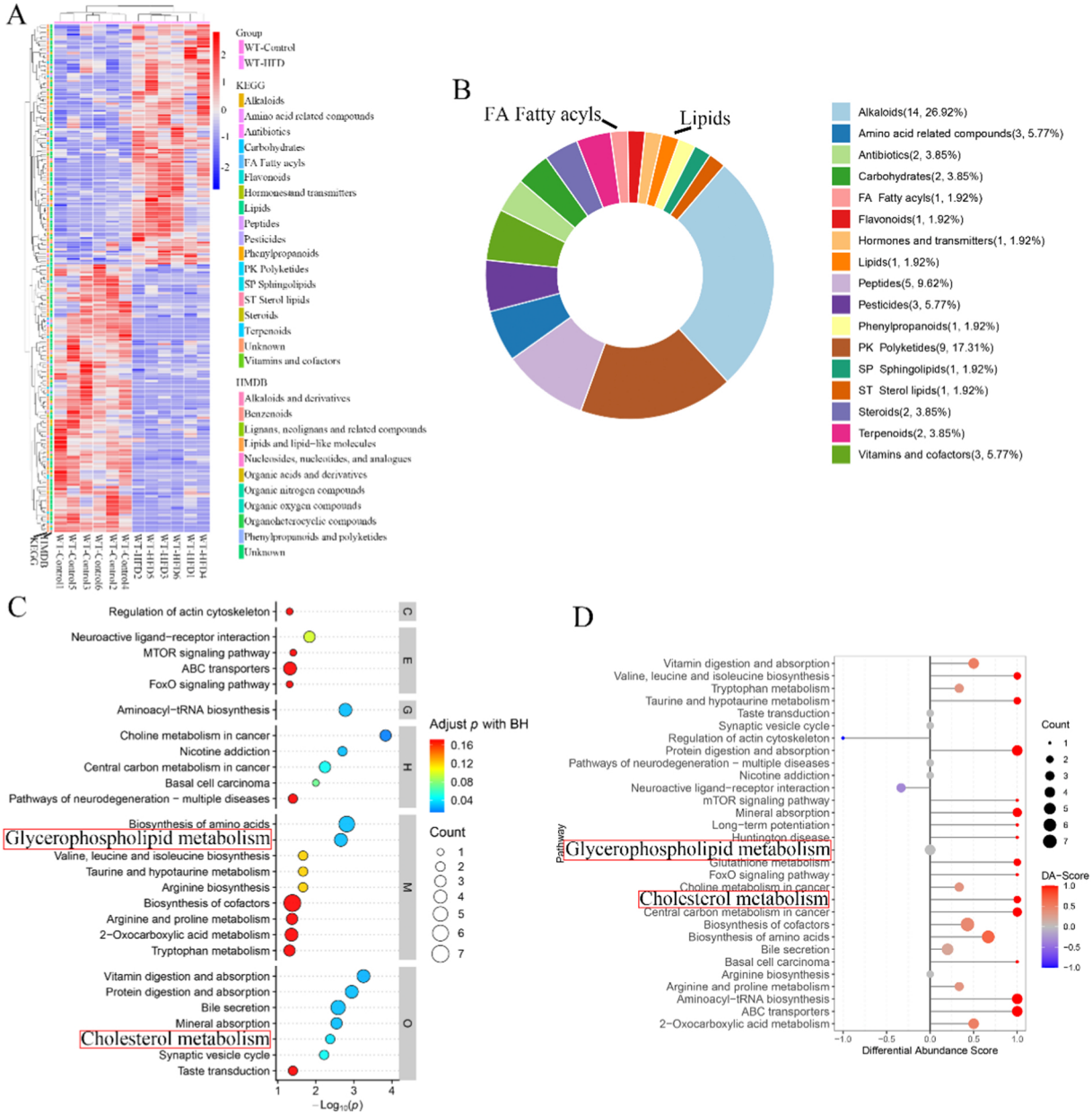
A
Group
WT-Control
WT-HTD
KEGG
Alkaloids
Amino acid related compounds
Antibiotics
Carbohydrates
FA Fatty acyls
Flavonoids
Hormones and transmitters
Lipids
Peptides
Pesticides
Phenylpropanoids
PK Polyketides
SP Sphingolipids
ST Sterol lipids
Steroids
Terpenoids
Unknown
Vitamins and cofactors
HMDB
Alkaloids and derivatives
Benzenoids
Lignans, neolignans and related compounds
Lipids and lipid-like molecules
Nucleosides, nucleotides, and analogues
Organic acids and derivatives
Organic nitrogen compounds
Organic oxygen compounds
Organoheterocyclic compounds
Phenylpropanoids and polyketides
Unknown
WT-Control1
WT-Control5
WT-Control3
WT-Control6
WT-Control2
WT-Control4
WT-HTD2
WT-HTD5
WT-HTD3
WT-HTD6
WT-HTD1
WT-HTD4
B
FA Fatty acyls
Lipids
Alkaloids(14, 26.92%)
Amino acid related compounds(3, 5.77%)
Antibiotics(2, 3.85%)
Carbohydrates(2, 3.85%)
FA Fatty acyls(1, 1.92%)
Flavonoids(1, 1.92%)
Hormones and transmitters(1, 1.92%)
Lipids(1, 1.92%)
Peptides(5, 9.62%)
Pesticides(3, 5.77%)
Phenylpropanoids(1, 1.92%)
PK Polyketides(9, 17.31%)
SP Sphingolipids(1, 1.92%)
ST Sterol lipids(1, 1.92%)
Steroids(2, 3.85%)
Terpenoids(2, 3.85%)
Vitamins and cofactors(3, 5.77%)
C
Regulation of actin cytoskeleton
Neuroactive ligand-receptor interaction
MTOR signaling pathway
ABC transporters
FoxO signaling pathway
Aminoacyl-tRNA biosynthesis
Choline metabolism in cancer
Nicotine addiction
Central carbon metabolism in cancer
Basal cell carcinoma
Pathways of neurodegeneration - multiple diseases
Biosynthesis of amino acids
Glycerophospholipid metabolism
Valine, leucine and isoleucine biosynthesis
Taurine and hypotaurine metabolism
Arginine biosynthesis
Biosynthesis of cofactors
Arginine and proline metabolism
2-Oxocarboxylic acid metabolism
Tryptophan metabolism
Vitamin digestion and absorption
Protein digestion and absorption
Bile secretion
Mineral absorption
Cholesterol metabolism
Synaptic vesicle cycle
Taste transduction
C
E
G
H
M
O
Adjust p with BH
0.16
0.12
0.08
0.04
Count
1
2
3
4
5
6
7
−Log10(p)
D
Vitamin digestion and absorption
Valine, leucine and isoleucine biosynthesis
Tryptophan metabolism
Taurine and hypotaurine metabolism
Taste transduction
Synaptic vesicle cycle
Regulation of actin cytoskeleton
Protein digestion and absorption
Pathways of neurodegeneration - multiple diseases
Nicotine addiction
Neuroactive ligand-receptor interaction
mTOR signaling pathway
Mineral absorption
Long-term potentiation
Huntington disease
Glycerophospholipid metabolism
Glutathione metabolism
FoxO signaling pathway
Choline metabolism in cancer
Cholesterol metabolism
Central carbon metabolism in cancer
Biosynthesis of cofactors
Biosynthesis of amino acids
Bile secretion
Basal cell carcinoma
Arginine biosynthesis
Arginine and proline metabolism
Aminoacyl-tRNA biosynthesis
ABC transporters
2-Oxocarboxylic acid metabolism
Pathway
Count
1
2
3
4
5
6
7
DA-Score
1.0
0.5
0.0
−0.5
−1.0
Differential Abundance Score

Figure 6

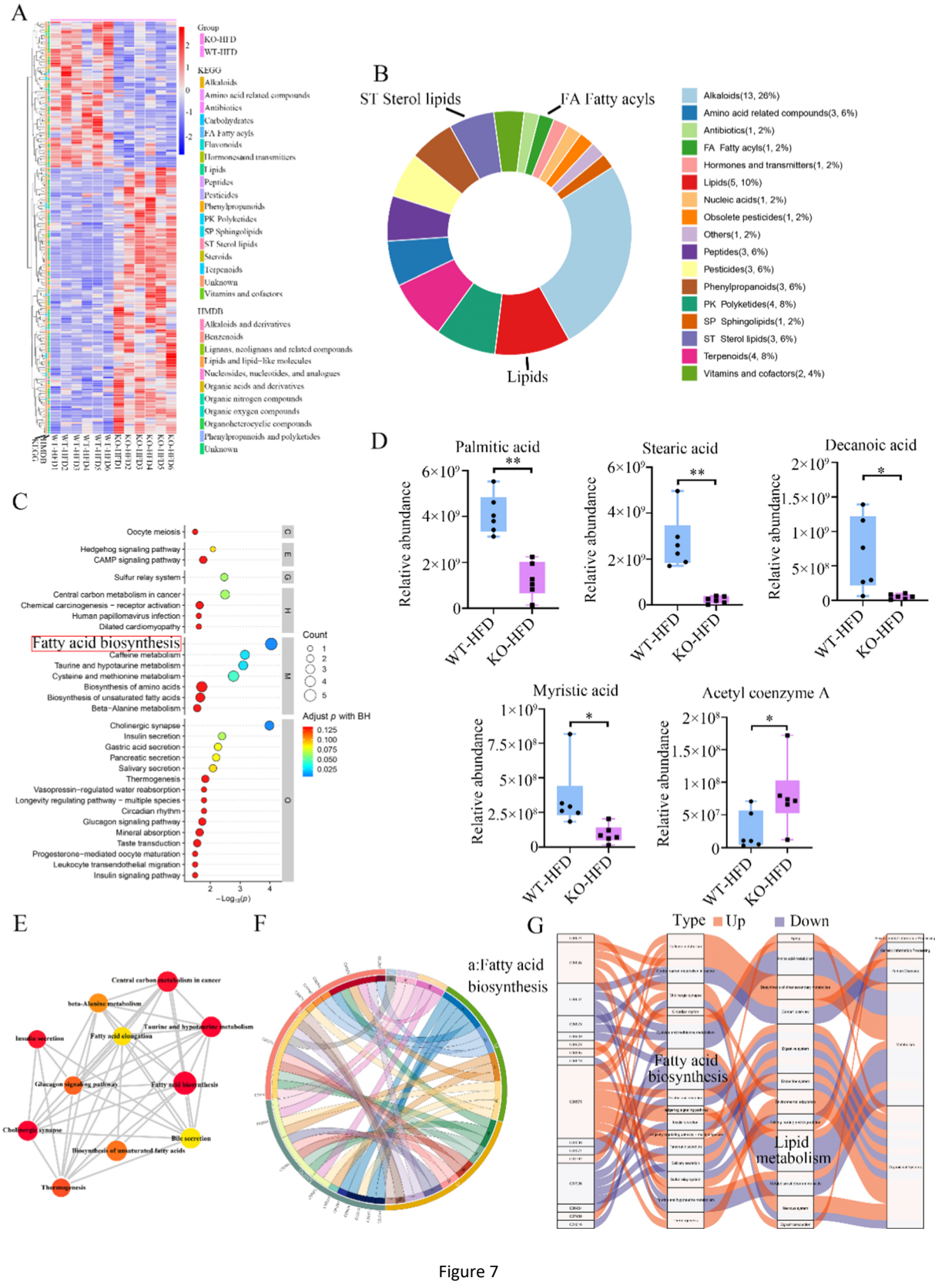
A
Group
KO-HFD
WT-HFD
KEGG
Alkaloids
Amino acid related compounds
Antibiotics
Carbohydrates
FA Fatty acyls
Flavonoids
Hormonesand transmitters
Lipids
Peptides
Pesticides
Phenylpropanoids
PK Polyketides
SP Sphingolipids
ST Sterol lipids
Steroids
Terpenoids
Unknown
Vitamins and cofactors
HMDB
Alkaloids and derivatives
Benzenoids
Lignans, neolignans and related compounds
Lipids and lipid-like molecules
Nucleosides, nucleotides, and analogues
Organic acids and derivatives
Organic nitrogen compounds
Organic oxygen compounds
Organoheterocyclic compounds
Phenylpropanoids and polyketides
Unknown
B
ST Sterol lipids
FA Fatty acyls
Lipids
Alkaloids(13, 26%)
Amino acid related compounds(3, 6%)
Antibiotics(1, 2%)
FA Fatty acyls(1, 2%)
Hormones and transmitters(1, 2%)
Lipids(5, 10%)
Nucleic acids(1, 2%)
Obsolete pesticides(1, 2%)
Others(1, 2%)
Peptides(3, 6%)
Pesticides(3, 6%)
Phenylpropanoids(3, 6%)
PK Polyketides(4, 8%)
SP Sphingolipids(1, 2%)
ST Sterol lipids(3, 6%)
Terpenoids(4, 8%)
Vitamins and cofactors(2, 4%)
C
Oocyte meiosis
Hedgehog signaling pathway
CAMP signaling pathway
Sulfur relay system
Central carbon metabolism in cancer
Chemical carcinogenesis - receptor activation
Human papillomavirus infection
Dilated cardiomyopathy
Fatty acid biosynthesis
Caffeine metabolism
Taurine and hypotaurine metabolism
Cysteine and methionine metabolism
Biosynthesis of amino acids
Biosynthesis of unsaturated fatty acids
Beta-Alanine metabolism
Cholinergic synapse
Insulin secretion
Gastric acid secretion
Pancreatic secretion
Salivary secretion
Thermogenesis
Vasopressin-regulated water reabsorption
Longevity regulating pathway - multiple species
Circadian rhythm
Glucagon signaling pathway
Mineral absorption
Taste transduction
Progesterone-mediated oocyte maturation
Leukocyte transendothelial migration
Insulin signaling pathway
Count
Adjust p with BH
−Log10(p)
D
Palmitic acid
Stearic acid
Decanoic acid
Myristic acid
Acetyl coenzyme A
Relative abundance
WT-HFD
KO-HFD
E
Central carbon metabolism in cancer
beta-Alanine metabolism
Taurine and hypotaurine metabolism
Insulin secretion
Fatty acid elongation
Glucagon signaling pathway
Fatty acid biosynthesis
Cholinergic synapse
Bile secretion
Biosynthesis of unsaturated fatty acids
Thermogenesis
F
G
Type
Up
Down
a:Fatty acid biosynthesis
Fatty acid biosynthesis
Lipid metabolism

Figure 7

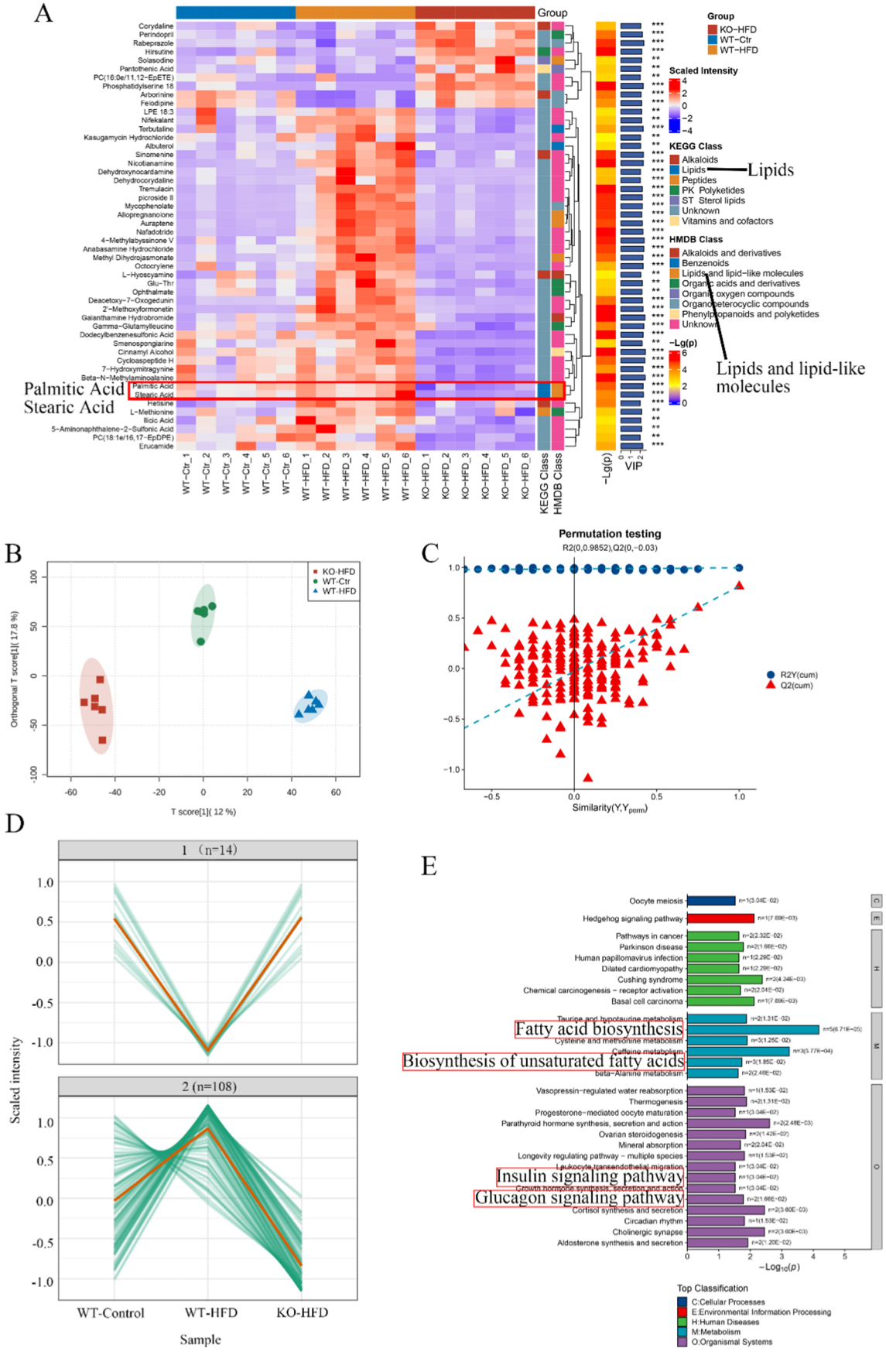
A
Group
KO-HFD
WT-Ctr
WT-HFD
Scaled Intensity
KEGG Class
Alkaloids
Lipids
Peptides
PK Polyketides
ST Sterol lipids
Unknown
Vitamins and cofactors
Lipids
HMDB Class
Alkaloids and derivatives
Benzenoids
Lipids and lipid-like molecules
Organic acids and derivatives
Organic oxygen compounds
Organoheterocyclic compounds
Phenylpropanoids and polyketides
Unknown
Lipids and lipid-like molecules
−Lg(p)
VIP
Palmitic Acid
Stearic Acid
Corydaline
Perindopril
Rabeprazole
Hirsutine
Solasodine
Pantothenic Acid
PC(16:0e/11,12-EpETE)
Phosphatidylserine 18
Arborinine
Felodipine
LPE 18:3
Nifekalant
Terbutaline
Kasugamycin Hydrochloride
Albuterol
Sinomenine
Nicotianamine
Dehydroxynocardamine
Dehydrocorydaline
Tremulacin
picroside II
Mycophenolate
Allopregnanolone
Auraptene
Nafadotride
4-Methylbyssinone V
Anabasamine Hydrochloride
Methyl Dihydrojasmonate
Octocrylene
L-Hyoscyamine
Glu-Thr
Ophthalmate
Deacetoxy-7-Oxogedunin
2'-Methoxyformonetin
Galanthamine Hydrobromide
Gamma-Glutamylleucine
Dodecylbenzenesulfonic Acid
Smenospongiarine
Cinnamyl Alcohol
Cyclosporeptide H
7-Hydroxymitragynine
Beta-N-Methylaminoalanine
Palmitic Acid
Stearic Acid
Hetisine
L-Methionine
Ilicic Acid
5-Aminonaphthalene-2-Sulfonic Acid
PC(18:1e/16,17-EpDPE)
Erucamide
WT-Ctr_1
WT-Ctr_2
WT-Ctr_3
WT-Ctr_4
WT-Ctr_5
WT-Ctr_6
WT-HFD_1
WT-HFD_2
WT-HFD_3
WT-HFD_4
WT-HFD_5
WT-HFD_6
KO-HFD_1
KO-HFD_2
KO-HFD_3
KO-HFD_4
KO-HFD_5
KO-HFD_6
KEGG Class
HMDB Class
B
KO-HFD
WT-Ctr
WT-HFD
Orthogonal T score[1](17.8 %)
T score[1](12 %)
C
Permutation testing
R2(0,0.9852),Q2(0,−0.03)
R2Y(cum)
Q2(cum)
Similarity(Y,Y$_{perm}$)
D
1 (n=14)
2 (n=108)
Scaled intensity
WT-Control
WT-HFD
KO-HFD
Sample
E
Oocyte meiosis
Hedgehog signaling pathway
Pathways in cancer
Parkinson disease
Human papillomavirus infection
Dilated cardiomyopathy
Cushing syndrome
Chemical carcinogenesis - receptor activation
Basal cell carcinoma
Taurine and hypotaurine metabolism
Fatty acid biosynthesis
Cysteine and methionine metabolism
Caffeine metabolism
Biosynthesis of unsaturated fatty acids
beta-Alanine metabolism
Vasopressin-regulated water reabsorption
Thermogenesis
Progesterone-mediated oocyte maturation
Parathyroid hormone synthesis, secretion and action
Ovarian steroidogenesis
Mineral absorption
Longevity regulating pathway - multiple species
Leukocyte transendothelial migration
Insulin signaling pathway
Growth hormone synthesis, secretion and action
Glucagon signaling pathway
Cortisol synthesis and secretion
Circadian rhythm
Cholinergic synapse
Aldosterone synthesis and secretion
C
E
H
M
O
−Log$_{10}$(p)
Top Classification
C:Cellular Processes
E:Environmental Information Processing
H:Human Diseases
M:Metabolism
O:Organismal Systems

Figure 8